

Pore-Structure Characterization of the Eocene Sha-3 Sandstones in the Bohai Bay Basin, China

Kaixun Zhang,^{*,†,‡,§} Yingchun Guo,^{*,†} Guoping Bai,[‡] Zongxiu Wang,[†] Bingda Fan,[§] Jianping Wu,[§] and Xinjie Niu[§]

[†]Institute of Geomechanics, Chinese Academy of Geological Sciences, Beijing 100081, China

[‡]State Key Laboratory of Petroleum Resources and Prospecting, China University of Petroleum, Beijing 102249, China

[§]Petrochina Huabei Oilfield Company, Renqiu, Hebei 062552, China

ABSTRACT: Mercury intrusion capillary pressure (MICP), nuclear magnetic resonance (NMR), routine core analysis, thin sections, and scanning electron microscope (SEM) analysis were used to gain insight into the pore structure of the Eocene Sha-3 (the third member of the Shahejie formation) low-permeability sandstones in the Raoyang sag, including pore type, pore geometry, and pore size. Quantitative NMR parameters and petrophysical properties were integrated to build up the relationship between microscopic pore structure and macroscopic performance. The pore systems of Sha-3 sandstones are dominantly of residual intergranular pores, intragranular dissolution pores, and intercrystallite micropores associated with authigenic clay minerals. The high threshold pressure and low mercury withdrawal efficiencies from MICP analysis indicate the poor pore connectivity and strong heterogeneous. Both uni- and bimodal transverse relaxation time (T_2) spectrum can be found because of the coexistence of small and large pores, and the T_2 of major pore size occurring at about 1.0 to 100 ms. The Sha-3 sandstones have a relatively high irreducible water content and short T_2 components in the T_2 range. Long T_2 components can only be observed in samples rich in large pores or microfractures. T_{2gm} (the geometric mean of the T_2 distribution) correlates well with irreducible water saturation and permeability. A methodology for pore structure classification is presented integrating NMR parameters of T_{2gm} , bulk volume of immovable fluid (BVI), and petrophysical parameters such as reservoir quality index (RQI) and permeability. Consequently, four types of pore structures (types A, B, C, and D) are identified, and characteristics of individual pore structure are summarized. The comprehensive analysis of NMR measurements combined with thin sections, SEM and MICP analysis is useful for describing microscopic pore structure, which is important to maintaining and enhancing petroleum recovery in low-permeability sandstone reservoirs.

1. INTRODUCTION

The Raoyang sag, famous for the discovery of the Renqiu Oilfield in 1975, is a prolific oil-producing province in Jizhong Depression of Bohai Bay Basin.^{1–3} Previous studies and exploration practice suggested the Eocene Shahejie formation in the Raoyang sag as effective source rocks and hydrocarbon-producing reservoirs.⁴ Recently, considerable hydrocarbons have been produced from the fan to braided deltaic sandstones in the Shahejie formation.^{2,3} Numerous studies, including depositional environments, geochemistry, diagenesis, and tectonic setting, have exhibited significant hydrocarbon potential in the Shahejie formation.^{2–6} The Eocene Shahejie formation was deposited in a lacustrine to fan-braided deltaic environment, and the lithology is dominated by deltaic fine–medium-grained sandstones interbedded with lacustrine dark-gray mudstones.^{1–3} Although formed in favorable tectonic setting and sedimentary facies,^{1,2} the Shahejie formation sandstones in the Raoyang sag are generally characterized by deep burial depth, low porosity, and ultralow permeability as well as strong heterogeneities due to the complicated deep-burial diagenesis.^{7,8} To help the successful exploration and efficient development of hydrocarbons in these low-permeability sandstones, the connection between micropore throat structures and macroscopic reservoir performances should be clarified^{9–12} because microscopic pore throat geometry controls the macroscopic petrophysical properties and petro-

leum charging, migration, and accumulation in low-permeability sandstones.^{13,14}

Laboratory nuclear magnetic resonance (NMR) measurements, which record the spin axis relaxation times (longitudinal being T_1 and transverse being T_2) of protons in the presence of pulsed and static magnetic fields,¹⁵ could directly provide the relaxation time distributions and consequently uncalibrated pore size distributions.^{16–18} Therefore, NMR measurements can be used to quickly and nondestructively characterize pore structure and fluid type and state in reservoir rocks.^{15,19} In addition, NMR measurements are widely used to determine fluid type and the proportion of fluid volumes and construct capillary pressure curves.^{15,20–24} Combined with thin sections, scanning electron microscopy (SEM), and mercury intrusion capillary pressure (MICP) measurements, NMR measurements can be used to construct pore size distribution, estimate macroscopic petrophysical property such as permeability, and quantitatively evaluate the complexity of pore structures.^{15,16,22,25–29} MICP analysis, which can measure pore throat size ranging from the micron scale to the nanoscale (about 3 nm),³⁰ is widely used for pore throat structure characterization in sandstones.^{31–34}

Received: November 23, 2017

Revised: January 18, 2018

Published: January 18, 2018

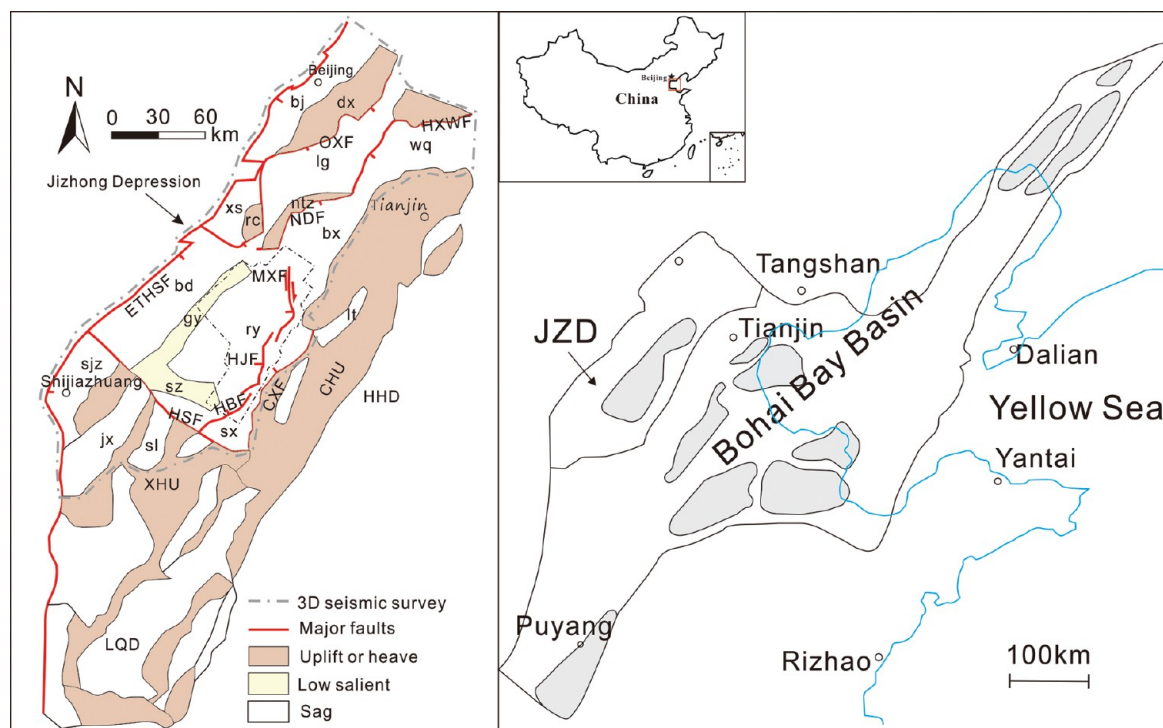


Figure 1. Location of the Bohai Bay Basin with the most petroliferous petroleum provinces highlighted by gray-colored areas.³

The main goals of this study are to improve our understanding of the pore structure of the Eocene Sha-3 low-permeability sandstone reservoir and provide insights into pore structure classification and evaluation using a combination of routine core analysis, thin section, SEM, MICP, and NMR measurements. The paper could be divided into six parts: (1) briefly describing the microscopic pore structure and macroscopic behaviors with thin section, SEM, and routine core analysis; (2) analyzing pore throat structure by MICP analysis and investigating the NMR T_2 spectrum; (3) quantitatively calculating NMR parameters including $T_{2\text{gmv}}$, $T_{2\text{cutoff}}$, bulk volume of immovable fluid (BVI) and free fluid index (FFI); (4) investigating the relationships between NMR parameters and petrophysical properties; (5) classifying and evaluating pore structure using the NMR analysis; and (6) summarizing the characteristics of various pore structures.

2. GEOLOGICAL SETTING

The Bohai Bay Basin, a typical Mesozoic and Cenozoic rifted lacustrine basin, is located in the eastern portion of the North China Craton, which is regarded as a hydrocarbon-resourcing basin in China.³⁵ The basin can be divided into six major sub-basins or depressions, including the Liaohe sub-basin in the northeast, the Jizhong sub-basin in the west, the Huanghua and the Jiyang sub-basins in the southeast, the Bozhong sub-basin in the east, and the Dongpu sub-basin in the southwest.^{3,6,36} The Jizhong depression is bounded by the Eastern Taihangshan fault to the west, the Cangxian uplift to the east, and the Xingheng uplift to the south³ (Figure 1). The Raoyang sag is a subtectonic unit lying in the southwest of the Jizhong depression, which is an important oil- and gas-producing province in East China. Besides the famous Renqiu oil field discovered in 1975, several large oil fields in the Raoyang sag have been discovered in recent years.³⁷ A total of four tectonic and sedimentary stages occurred in the Raoyang sag, including extension and deep subsidence, uplifting,

extension and depression, and shrinkage and extinction.³⁸ The Eocene and Neocene strata consist of the Kongdian formation (Ek), the Eocene Shahejie formation (Es) and the Dongying Formation from bottom to top.³⁹ The Eocene Shahejie formation, which contains abundant hydrocarbon resources, can be divided into four members vertically from bottom to top based on the lithological association and sedimentary cycles, including first, second, third and fifth members (Es1, Es2, Es3, and Es4).² The underlying Sha-4 (Es4) and Sha-3 (Es3) members are mainly source rocks, whereas the Sha-1 member is composed partly of source rocks.⁶ The Sha-3 members, which are the main objects of this study, was deposited in a lacustrine-delta environment, consists of both reservoirs and organic-rich source rocks.⁴⁰ The reservoirs are dominated by fine–medium-grained sandstones of a fan-braided delta environment, whereas the source rocks is mainly the lacustrine gray to dark-gray mudstones.^{41,42}

3. ANALYTICAL METHODS

A total of 40 representative core plugs (about 1 in. in diameter and 2 in. in length) of the Eocene Sha-3 sandstones were taken from 11 petroleum exploration wells, including the Liu 99 well, Liu 101 well, Chu 22 well, Liu 425, Liu 498, Chushen 1, Liu 446, Liugu 2, etc. These samples were subjected to a laboratory workflow including: (1) mineralogy and thin section analysis, (2) porosity and permeability measurements, (3) SEM analysis to determine pore systems and clay minerals, (4) MICP analysis, and (5) NMR measurements.

Routine core analysis (grain density, porosity, and permeability) was performed on 140 core plugs with the aim to characterize the flow potential (permeability) and the storage capacity (porosity) of the reservoir. The He porosity and permeability were measured using the CMS-300 instrument at a net confining pressure of 800 psi.

To identify clay minerals and corresponding pore characteristic, e.g., pore spaces, pore throat type, and pore throat radius, a total of eight freshly broken rock fragments were coated with a thin layer of carbon and examined with the S-4800 scanning electron microscope (SEM) equipped with a backscattered electron (BSE) detector.

Thin sections (30 μm in thickness), which were impregnated with blue-dye resin to highlight porosity, were point-count analyzed (300 points per sample) under plane-polarized and cross-polarized light to determine the volume and distribution of intergranular and intra-granular porosity. Thin sections were also stained with Alizarin Red S and potassium ferricyanide for the recognition of Fe-dolomite, Fe-calcite, and nonferroan calcite.

MICP analyses were performed on 40 core samples (25 \times 50 mm columnar samples) to determine the pore structures and pore throat distribution at the laboratory of China University of Petroleum (Beijing). The 9505 mercury injection apparatus applied to this experiment of which the maximum mercury injection pressure is 151.07 MPa.

NMR T_2 relaxation time was used to determine the pore size distribution and calculate the NMR porosity, irreducible water, and mobile water content as well as to estimate the permeability. To determine the transversal relaxation time (T_2) distributions of saturated and centrifuged (unsaturated) samples, including incremental and cumulative T_2 values, a set of 41 core samples was prepared for laboratory NMR measurements in State Key Laboratory of Petroleum Resources and Prospecting of China. The NMR apparatus (Maran-2 ultrarock spectrometer produced by Oxford Instruments) provides 2 M HZ frequency of magnetic field, waiting time of 15 000 ms, and echo spacing T_e of 0.3 ms. The measurement was conducted under temperature of 25 $^\circ\text{C}$. A total of 128 stacks were performed to obtain the relaxation time distribution. The samples were first fully saturated with NaCl brine with a salinity of 50 000 mg/L at a net confining pressure of 20 MPa for 48 h, and then the T_2 distributions at this saturated status were measured. After that, the free water in core plugs was removed by keeping samples in a centrifugal machine with a rotation speed of 10 000 r/min for 1 h. The T_2 distributions (incremental and cumulative) of these samples were measured again at the centrifuged status.

4. RESULTS

4.1. Microscopic Pore Systems and Macroscopic Performances. The routine core analysis of the 140 core samples show that the permeability ranges from 0.012 mD to 61.03 mD, while porosity varies between 2.06% and 19.9% with an average value of 11.9% (Figure 2). Even variations in

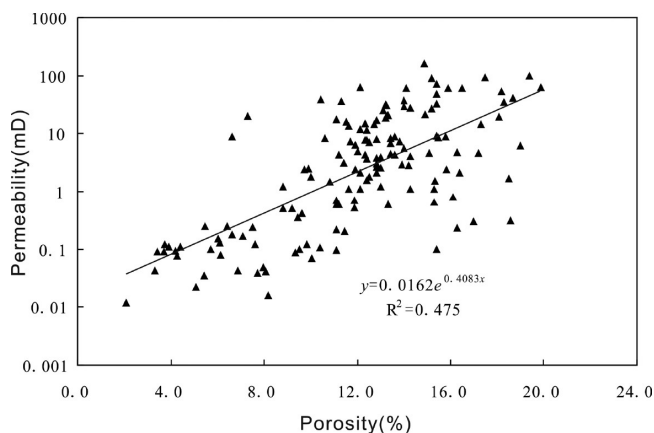


Figure 2. Cross-plot of porosity vs permeability for the Shahejie sandstones in the Raoyang sag.

permeability of 4 orders of magnitude can be observed for the same porosity (Figure 2). A large portion of samples are characterized by high porosity but low permeability or low porosity but high permeability, indicating that the permeability is generally unrelated to the total porosity but rather controlled by pore throat structures (pore and throat types, radius, and pore connectivity; Figure 2). Samples characterized by high porosity

but low permeability are interpreted to have abundant microporosity and poorly connected pores (Figure 2). In contrast, the high-permeability but low-porosity samples have large pore throat radius and may contain microfractures.^{12,43} The low correlation coefficient between permeability and porosity ($R^2 = 0.47$) gives additional evidence for the heterogeneous nature of the pore throat structures (Figure 2).

Thin section observations and SEM analysis suggest that that pore systems of Sha-3 sandstones in the Raoyang sag are dominantly of residual intergranular pores, intragranular dissolution pores, or even moldic pores. The residual intergranular pores, which are of primary origins and irregular shapes, are predominantly in coarser-grain sized and well-sorted samples (Figure 3A,B). The secondary dissolution pores can be found in some samples, which were resulted from partial to complete dissolution of framework grains such as feldspars (Figure 3C). Thin section analysis (presence of blue epoxy) also indicates that abundant intragranular pores occur in feldspars and rock fragments (Figure 3D). The secondary intergranular pores commonly coexist with the intergranular ones² (Figure 3C,D). Moldic pores due to complete dissolution of the framework grains can be occasionally observed (Figure 3E). Porosity could be quantified through thin section point-counting analysis, and also checked against routine core analysis.⁴⁴ Total thin-section porosity of the sandstones, reveals a wide range from trace levels (<1%) to 14.50% with an average of 7.5%. Thin section analysis reveals that the clean sandstones do not contain abundant micropores (<10 μm) (Figure 3A,B). In contrast, samples with low porosity have relative high content of micropores.

The presences of micropores in the Sha-3 sandstones in the Raoyang sag can also be confirmed by the SEM analysis. In fact, there are many micropores, which are below the resolution of the microscopic thin section analysis, can be detected by the SEM analysis. For instance, abundant honeycomb-like micropores in feldspars (Figure 3F) and intercrystalline micropores associated with authigenic clay minerals, e.g., illite (Figure 3G), and mixed layered illite and smectite (Figure 3H) can be observed in SEM images.⁸ Microfractures detected by both thin-section and SEM images, are also important pore spaces in Sha-3 low-permeability sandstones (Figure 3I,J).

4.2. Pore Throat and Pore Size Distributions. Reservoir porosity and permeability are macroscopic expressions of pore structure that integrate geometry (pore throat size and shape and pore size distribution) and topology (pore connectivity).¹⁰ In this section, MICP analysis and NMR measurements are used to identify pore throat and pore size distributions of Sha-3 low-permeability sandstones.

Pore networks of sandstone in MICP analysis refer to pores connected through by pore throats.^{46–48} Typical capillary pressure curves of Sha-3 low-permeability sandstones commonly exhibit a gradual increase in mercury saturation with capillary pressure⁴⁸ (Figure 4). Importantly, the capillary curves of these sandstone samples indicate the variation of reservoir quality and microscopic complexity of pore structures, as well as heterogeneous pore networks. As can be seen from Figure 4, samples are characterized by moderate to high threshold pressures with the maximum mercury saturation of 25%–90% at the maximum injection pressure 151.07 MPa. In terms of the Sample A, the maximum mercury saturation is 92%, and the threshold pressure is low to moderate (2.1 MPa); additionally about 45% of mercury resided at the end of the extrusion (capillary pressure was gradually decreased to zero) (Figure 4A). In terms of sample D, only 26.6% of the pore volumes are

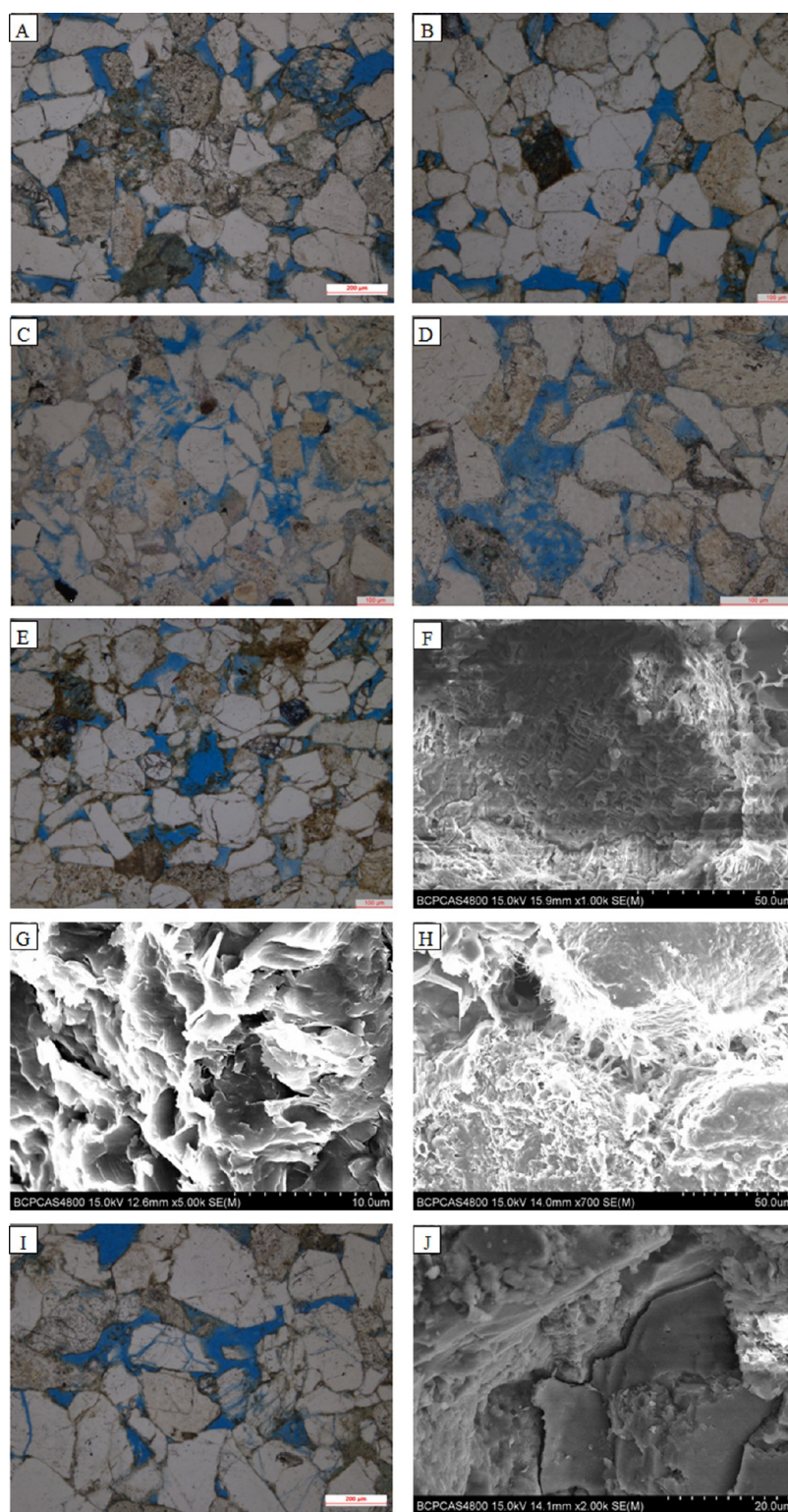


Figure 3. Photomicrographs showing the pore systems of the Sha-3 sandstones in the Raoyang sag. (A) Intergranular pores highlighted with red-dye resin, Liu 101, 3-106. (B) Intragranular pores, Liu 101, 3-126. (C) Secondary dissolution pores, Liu 101, 3-101. (D) Microfracture, Liu 101, 3-101. (E) Moldic pores, Liu 101, 3-99. (F) Micropores associated with feldspar dissolution, Liu 101, 3707m. (G) Illite abundant in intercrystalline micropores, Liu 101, 3634.22m. (H) Illite and the mixed layered illite and smectite abundant in micropores, Liu 101, 3691.94m. (I) Microfracture, Liu 101, 3-107. (J) Microfracture, Liu 101, 3522.95m, SEM.

saturated with mercury at the maximum injection pressure (Figure 4), indicating poor pore connectivity. Furthermore, more than half of the injected mercury is resided at the end of the extrusion, which can be attributed to the presence of ink-bottle-

shaped pores, i.e., pore geometries composed of a system of large body pores but interconnected by very narrow throats.^{49–51} Therefore, the low mercury withdrawal efficiencies give additional evidence to the poor connectivity of pore systems. The

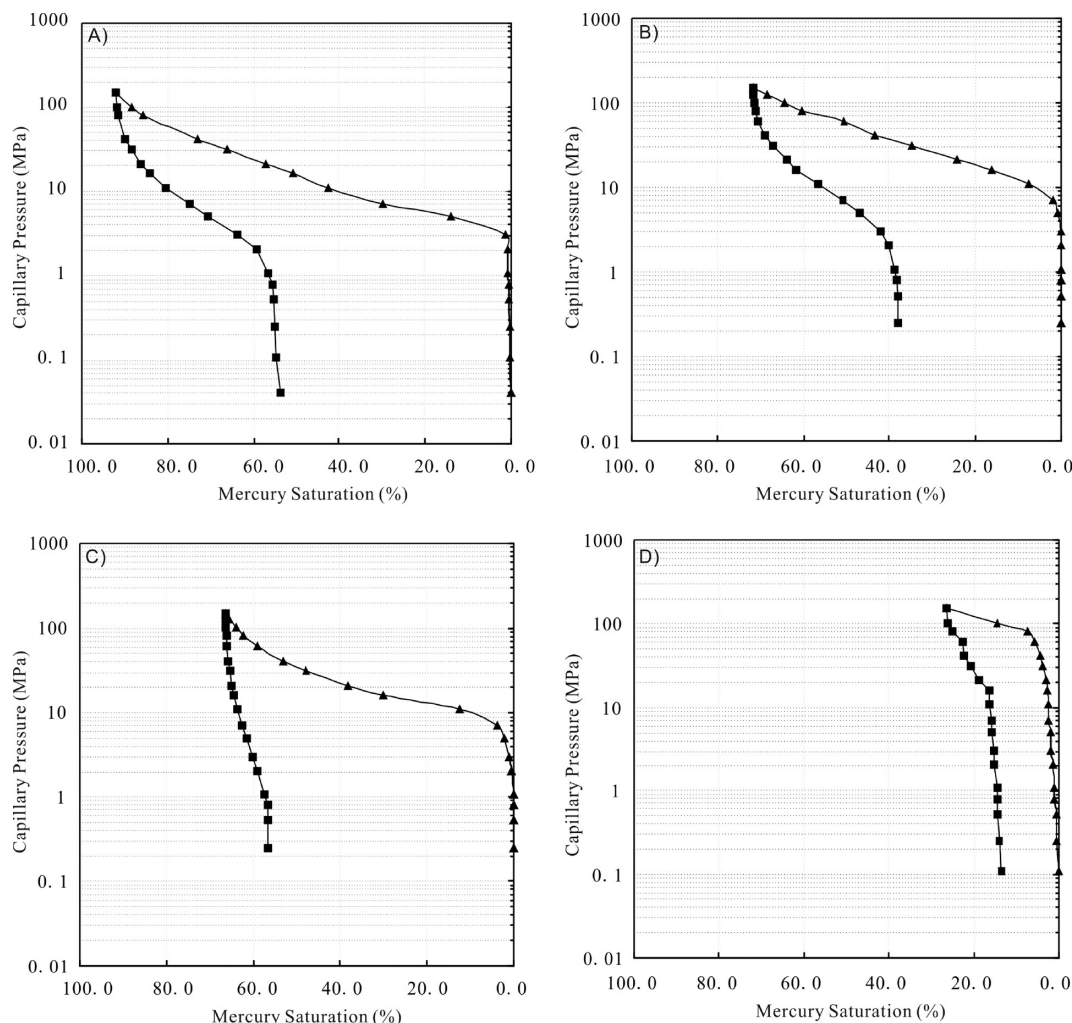


Figure 4. Typical capillary pressure curves of the Sha-3 sandstones in the Raoyang sag.

transitional pore structure types are presented in Figure 4B,C. As can be observed from Figure 4, the maximum mercury saturation gradually decreases from sample A to sample D, whereas the threshold pressure gradually increases; additionally, more and more content of mercury resided at the end of the extrusion, and this implies that the microscopic pore structure and macroscopic reservoir quality become more complex and poorer from sample A to sample D (Figure 4).

MICP is sensitive to pore throat sizes rather than pore body sizes,¹⁵ while NMR relaxation time distributions are directly determined by pore size distributions with the assumption that majority of the pore volume is composed of pore bodies.^{15,17} The T_2 decay rates are mainly controlled by the surface-to-volume ratio and pore size: short T_2 value indicates small pores and a large surface-to-volume ratio, whereas long T_2 means a small surface-to-volume ratios and, therefore, large pores.⁵² NMR porosity measured in the NMR measurements follows a good linear trend with increasing water porosity trend (Figure 5A), while the high coefficient correlation ($R^2 > 0.98$) suggests a good relationship between NMR porosity and He porosity (Figure 5B). Therefore, the NMR analysis can measure almost the entire pore systems saturated with the brine. However, it should be noted that not all pore systems can be saturated with 100% brine, even when they were kept at a confining pressure of 20 MPa for 1 h. As can be seen from Figure 5B, there are some data points

below the “unit slope line” ($y = x$), which indicates that some micropores may not be saturated with brine due to the poor connectivity of pore systems.

The incremental and cumulative T_2 spectrum (transversal relaxation time distribution) in Figure 6 provide significant information about the interactions between pore fluids and grain surfaces and, therefore, pore structure.^{12,53} The NMR relaxation time distributions of saturated sample range from 0.1 to 1000 ms with corresponding T_2 of major pore size occurring at about 1.0 to 100 ms (Figure 6). In NMR measurements, the pore systems are classified into small pores with irreducible water and large pores holding movable fluids and contributing to the flow system.¹² The capillary and clay-bound irreducible water (BVI) in small pores can be separated from the FFI in large pores using a NMR parameter, named $T_{2\text{cutoff}}$.^{22,41,53,54} By the drawing of a horizontal projection line from the centrifuged cumulative curve, the intersection of this projection line at the saturated cumulative curve could be used to determine the $T_{2\text{cutoff}}$ value (Figure 6).^{22,54} The $T_{2\text{gm}}$ can be calculated as the amplitude weighted mean on a logarithmic scale.¹²

The cumulative T_2 distributions for saturated status display unimodal and bimodal behaviors, which represents a geometrical arrangement composed of small to large pore size domains. About 75% of the samples are characterized by bimodal T_2 distributions (Figure 7A), indicating the variation of pore sizes

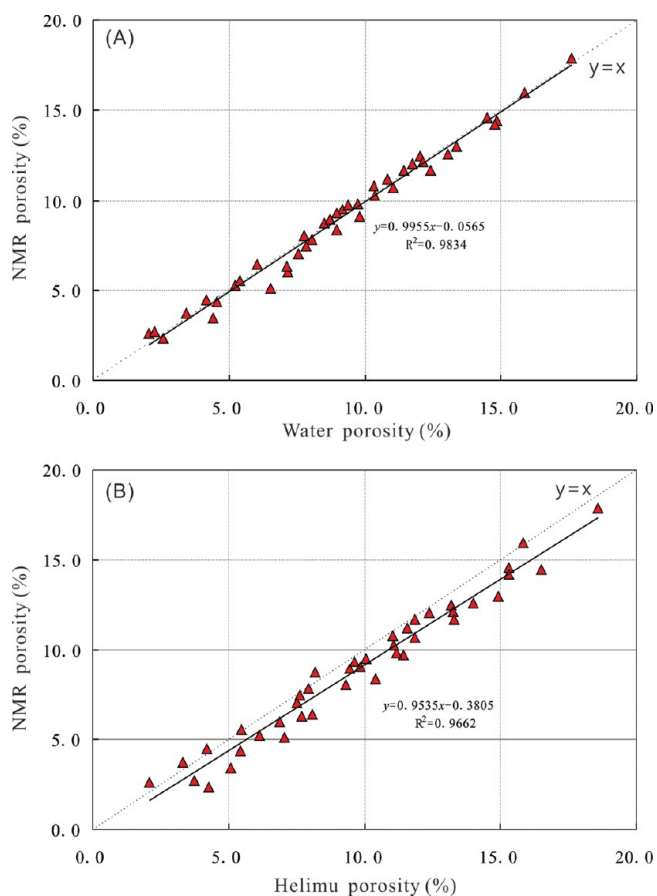


Figure 5. Plot of (A) NMR porosity vs water porosity and (b) NMR porosity vs helium porosity of the Sha-3 sandstones in the Raoyang sag.

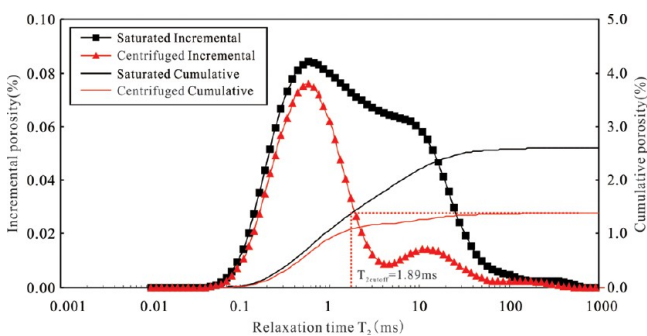


Figure 6. NMR T_2 incremental and cumulative spectra.

and the coexistence of small pores and large pores, which is agreement with the thin section observation and SEM analysis. The wide range of pore sizes in the Sha-3 heterogeneous sandstones contributes to the bimodal T_2 spectrum (Figure 7A). The bimodal T_2 distributions can be divided into two parts: a short component (T_{2s}) associated with the presence of micropores in clay minerals and capillary pore sizes and a long component (T_{2l}) corresponding to the large intergranular pores and microfractures^{12,53} (Figure 7A). Lacking of the macropores in the low-permeability sandstones, the main T_2 component appears as a major dominant peak at the shorter T_2 times, and there are minor peaks or a tail distribution of T_2 large than 300 ms that are most likely associated with the remaining larger pores²⁸ (Figure 7A). However, long T_2 components can be observed in

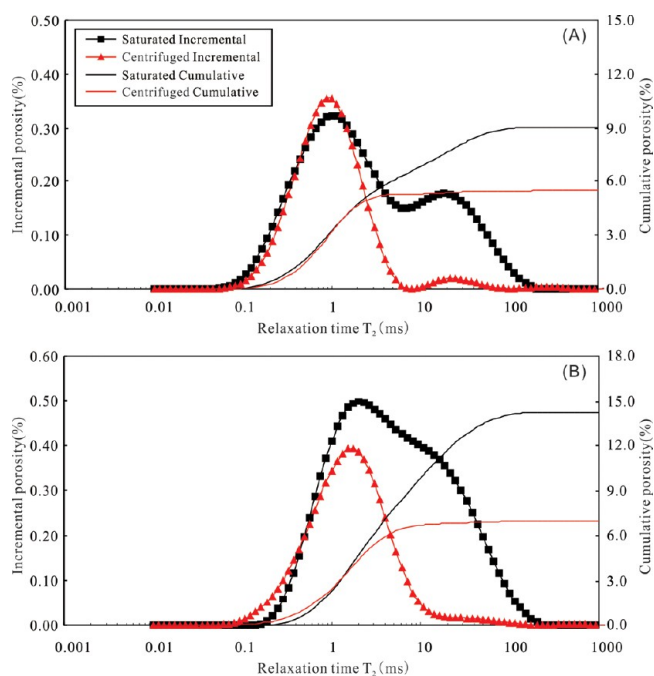


Figure 7. NMR T_2 incremental and cumulative spectra with bimodal behavior and unimodal behavior, respectively.

samples with microfractures, and there are tail distributions of T_2 relaxation time larger than 100 ms.^{12,55}

The unimodal T_2 behaviors refer to the T_2 spectrum of only one representative modal with no or weak T_{2l} components (Figure 7B). No evident tail distributions and long T_2 components greater than 100 ms, which are associated with the large pores or microfractures, can be observed. In contrast, the high content of short relaxation time components suggest abundant poorly connected micropores, which correspond to the short relaxation time components in the T_2 distribution, and these micropores have a great effect on the heterogeneity.¹² High irreducible water content and low movability of water of samples resulted in NMR signal amplitudes with no evident deviation under saturated and centrifuged conditions (Figure 6).

The NMR measurements performed on 40 samples show that the $T_{2\text{cutoff}}$ ranges from 1.04 to 43.29 ms, with an average value of 12.5 ms. The BVI values vary significantly from 31.49% to 97.93%, with an average value of 65.42%, which means more than half of the pore systems are associated with clays minerals and within capillary pore sizes. The high BVI content indicates poor connectivity and complicated pore systems. The $T_{2\text{gm}}$ parameter, which is the geometric mean of the NMR T_2 distribution, is in the range from 0.62 to 44.03 ms and averaged as 8.12 ms. Generally, the macroscopic reservoir quality and the microscopic pore structure are positively related to the $T_{2\text{gm}}$, whereas a moderate to strong negative relationship occurs between BVI and $T_{2\text{gm}}$ with a correlation coefficient (R^2) of 0.77, which indicates that a large proportion of micropores can result in a low $T_{2\text{gm}}$ value and, therefore, a high irreducible water content (Figure 8A). Furthermore, a high exponential relationship (R^2 of 0.78) between permeability and $T_{2\text{gm}}$ (Figure 8B) indicates that samples with high permeability tend to have more large pores and, therefore, high content of long- T_2 components (Figure 8B). Thus, $T_{2\text{gm}}$ is a sensitive NMR parameter for both the microscopic pore structure and the macroscopic petrophysical properties.

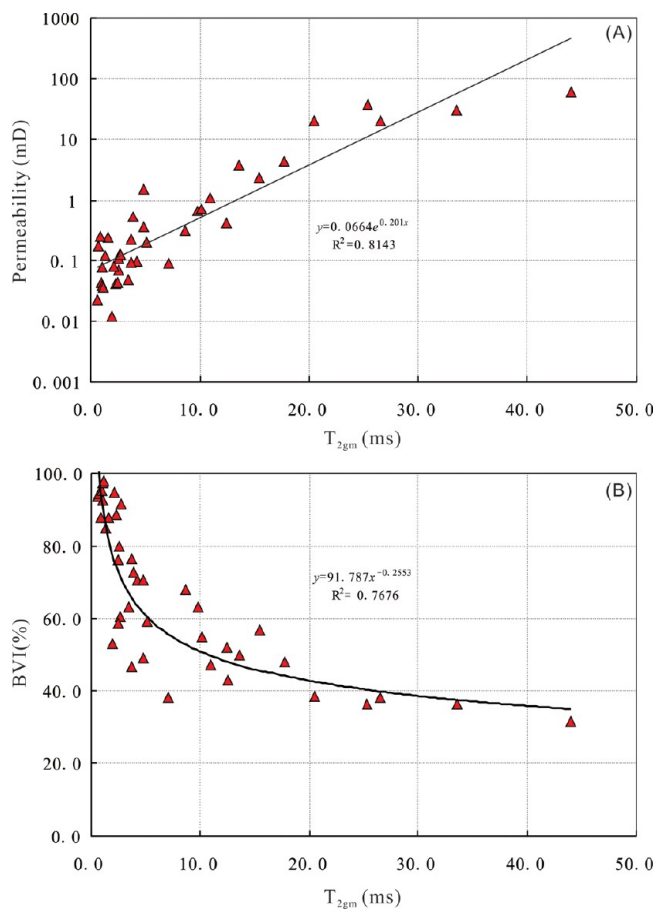


Figure 8. Plot of (A) permeability vs T_{2gm} and (B) BVI content vs T_{2gm} of the Sha-3 sandstones in the Raoyang sag.

5. DISCUSSIONS

Because low-permeability sandstones commonly are characterized by complicated microscopic pore structures and various pore types and multiscale pore sizes,^{20,54,56–58} pore structure classification and evaluation is significant for sweet-spot prediction and production optimization.^{51,59,60} Previous studies from Coates et al.,⁶¹ Ge et al.,²² Lai et al.,¹² Daigle and Johnson,¹⁷ and Zhao et al.¹⁸ suggested that NMR measurement is an important approach for pore structure classification and evaluation of low-permeability sandstones reservoirs because NMR could nondestructively determine porosity, pore size distributions and estimate permeability.

The parameter of reservoir quality index (RQI) is introduced here for pore structure classification and evaluation, has an advantage in addressing the reservoir quality in various scales,⁶² and is one of the best macro physical parameter for quantitative characterization of microscopic pore structure.⁶³ As an important parameter for hydraulic flow unit theory,^{12,18} it is defined as the ratio of permeability to fractional porosity under the square root⁶⁴ (eq 1). RQI is one of the best macro physical parameter for quantitative characterization of microscopic pore structure.⁶³ Generally, the microscopic pore structure has a positive trend with the increasing RQI values:¹²

$$RQI = \sqrt{\frac{K}{\phi}} \quad (1)$$

where RQI is reservoir quality index in micrometers, K is the permeability in square micrometers, and ϕ is the fractional porosity.

Regression analysis shows that RQI is strongly correlated with T_{2gm} with a high correlation coefficient (R^2) of 0.89 (Figure 9).

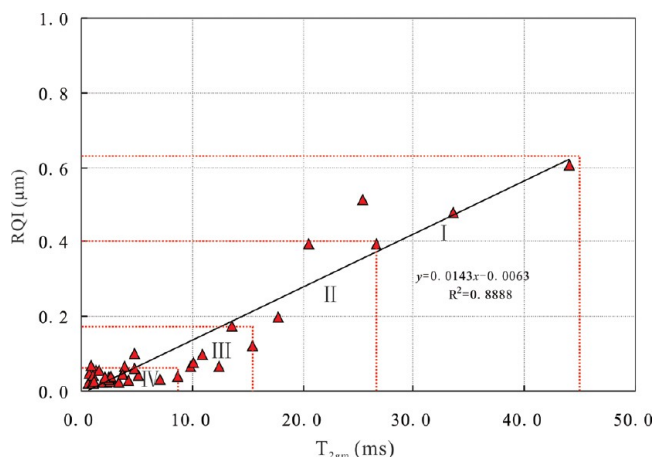


Figure 9. Plot of RQI vs T_{2gm} of the Sha-3 sandstones in the Raoyang sag.

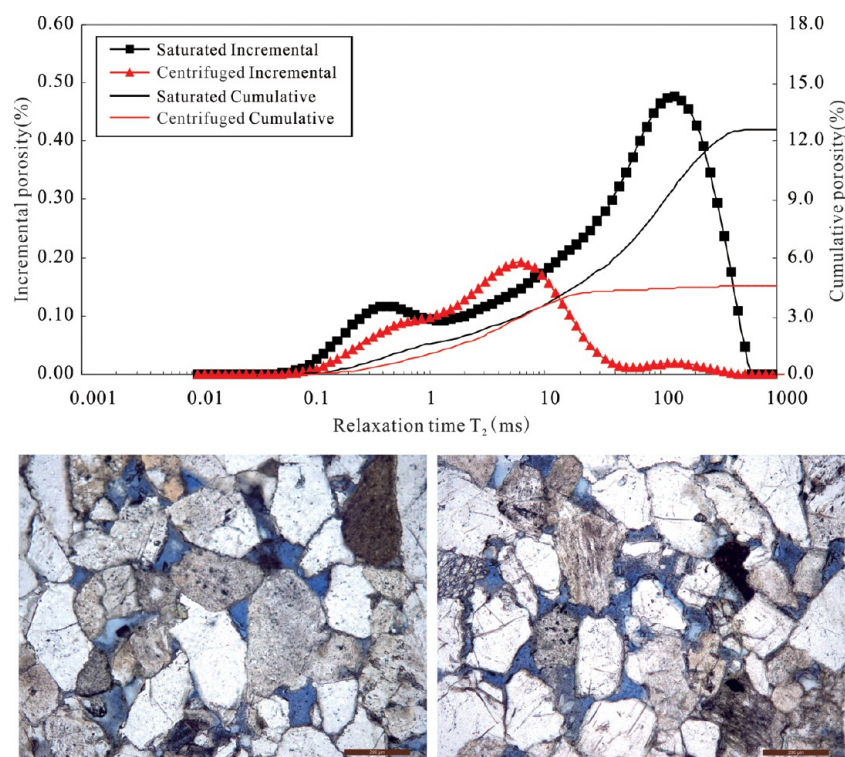
Previous study also confirmed that the NMR parameter T_{2gm} could be used for the characterization of pore structure and reservoir quality index.^{12,18,32} In this study, the T_{2gm} is integrated with the RQI as well as permeability to comprehensively characterize and classify pore structures in Sha-3 sandstones in the Raoyang sag. The classification standards for pore structure based on NMR parameters and reservoir quality are presented in Table 1 and Figure 9. A total of four types of pore structures are identified on the basis of the NMR parameters (BVI and T_{2gm}) and petrophysical parameters (permeability and RQI; Table 1 and Figure 9).

The T_2 spectrum of type A pore structure is characterized by a wide spectrum, a bimodal behavior as well as obvious right-skewed distribution (lower left peak but higher right peak) (Figure 10). Samples with type A pore structure commonly have high permeability and low immobile water (Table 1). Large residual intergranular pores or moldic pores are typical type A pore structures, which are connected by large pore throats and can make a significant contribution to permeability (Figure 10).^{11,45,65,66} Therefore, type A pore structure may have a highest maximum mercury saturation and relatively high efficiency of mercury withdrawal (Figure 4A), which implies a good pore connectivity. Also, microfractures in some samples result in high core-measured permeability. Due to the presences of large intergranular pores and microfractures, abundant long T_2 components can be observed, and minor peaks associated with small pores are present. Therefore, the irreducible water content will be low. In some cases, long T_2 tails can be observed with main peak at T_2 values higher than 100 ms (Figure 11). High content of movable water makes the NMR signal amplitudes under saturated and centrifuged conditions deviate significantly (Figures 10 and 11) because most of movable water can be removed by the centrifugal machine.

The NMR T_2 spectrum of type B pore structure has a wide range from 0.1 to 700 ms; however, they may show unimodal behaviors (Figure 7B) or bimodal behaviors (Figure 12). The main peaks of the T_2 spectrum occur at T_2 between 10 and 100 ms (Figure 12). Although long T_2 components occur in type B

Table 1. Classification Standard of Pore Structure of Sha-3 Sandstones Based on NMR Parameters and RQI

pore structure	NMR parameters		petrophysical parameter			pore systems
	T_{2gm} (ms)	BVI (%)	porosity (%)	permeability (mD)	RQI (μm)	
A	>26	<40.0	>15.0	>10.0	>0.40	microfracture or abundant in large intergranular pores
B	15.0–26.0	40.0–50.0	10.0–15.0	1.0–10.0	0.18–0.40	coexistence of large intergranular pores and secondary dissolution pores
C	9.0–15.0	50.0–65.0	5.0–10.0	0.1–1.0	0.03–0.18	rare in large intergranular pores but abundant in dissolution pores or micropores
D	<9.0	>60.0	<5.0	<0.1	<0.03	dominantly of micropores

Figure 10. Typical T_2 spectrum of type A pore structure of the Sha-3 sandstones in the Raoyang sag.

pore structures, short T_2 components can be found in some samples, which is attributed to the existence of irreducible water (Figure 12). Type B pore structures are generally characterized by high permeability of 1 to 10 mD but a moderate BVI value. Type B pore structures also have a high maximum mercury saturation and relatively high efficiency of mercury withdrawal (Figure 4B), which indicates that more than 70% of the pore throat systems can be invaded by mercury at the maximum injection pressure. Different from type A pore structures, type B pore structures have much-lower full NMR signal (especially the right peak representing the large intergranular pores) without the occurrence of tail (Figures 10 and 12). This pore system is characterized by the coexistence of large intergranular pores and secondary dissolution pores or micropores (Table 1 and Figure 12).

The NMR T_2 spectrum of type C pore structure has a relatively small range of 0.1 to 100 ms. The pore system is dominated by secondary dissolution pores or poorly connected micropores, thus exhibiting a bimodal and left-skewed (higher left peak but lower right peak) T_2 spectrum with the main peaks at T_2 of 1 to 10 ms (Figure 13). Weak T_{2l} components are presented; in contrast, strong T_{2s} components imply the high content of immovable water (BVI) existing in the micropores (Figure 13).

Type C pore structure commonly has a high immobile water content larger than 50% but a low permeability between 0.1 to 1 mD (Table 1 and Figure 13). Therefore, a type C pore structure has a low to moderate maximum mercury saturation and low efficiency of mercury withdrawal (Figure 4C), indicating that most of the pore systems are not connected by effective throats.

The NMR T_2 spectrum of type D pore structures has a very narrow range from 0.1 to 100 ms, which is similar to that of type C pore structures. The one distinct peak (unimodal behavior) indicate a relatively continuous pore size distribution (Figure 14). The intercrystalline micropores, which are associated with the various types of clay minerals, are the predominant pore types in this type of pore structure. Extremely high immovable water but low permeability (<0.1 mD) occurs in this pore structure due to the poor connectivity of the pore systems. Type D pore structure also has the lowest maximum mercury saturation and highest threshold pressure (Figure 4D), indicating that the poorest pore connectivity. Additionally, the total NMR signal amplitudes under saturated and centrifuged conditions have no evident deviations (Figure 14) because most of the irreducible water cannot be removed by the centrifugal machine, even with a

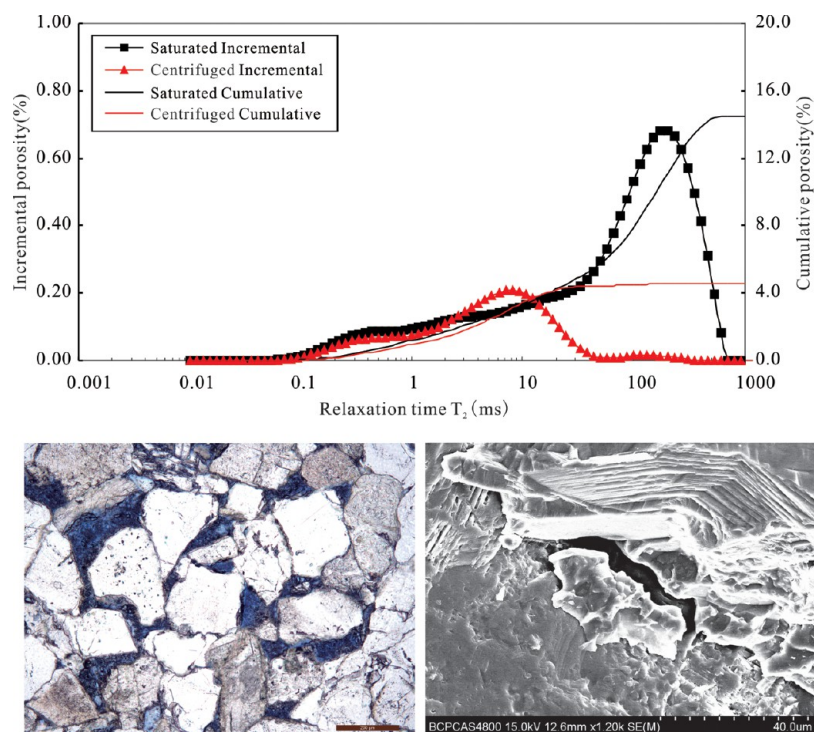


Figure 11. Typical T_2 spectrum of type A pore structure (with microfractures).

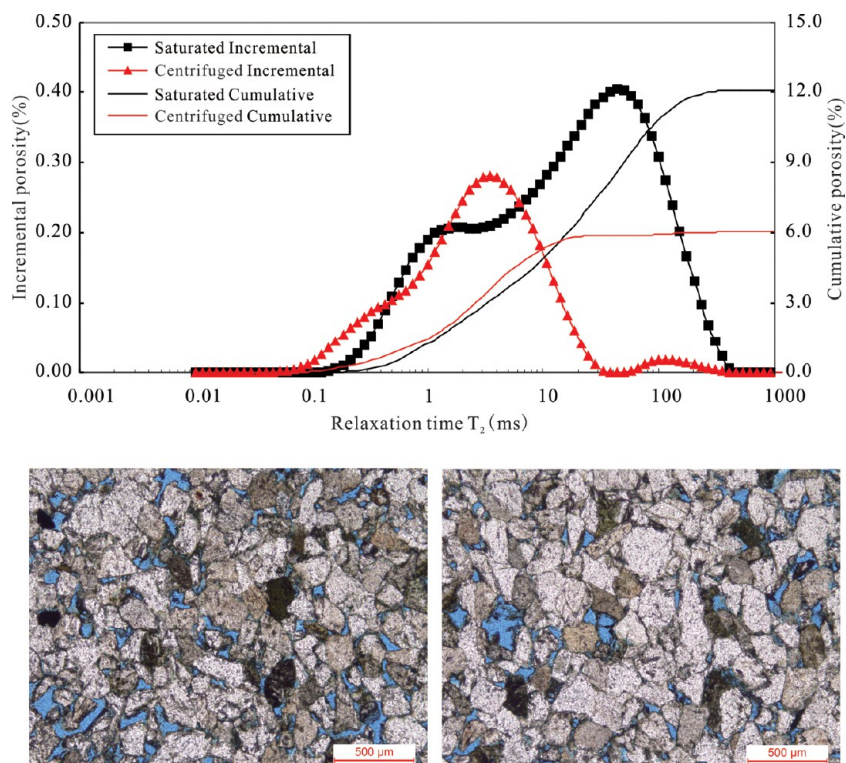


Figure 12. Typical T_2 spectrum of type B pore structure of the Sha-3 sandstones in the Raoyang sag.

rotation speed of 10 000 r/min for 1 h, and this gives additional evidence to the poor pore connectivity.

6. CONCLUSIONS

Thin section observations and SEM analysis show that that pore systems of Sha-3 sandstones are primarily residual intergranular pores, intragranular dissolution pores, or moldic pores. The

differences of core-measured porosity and thin-section porosity suggest considerable micropores. SEM analysis confirms abundant honeycomb-like micropores in feldspars and intercrystalline micropores associated with the authigenic clay minerals. The threshold pressure of pore samples are moderate to high with relatively low maximum mercury saturation at the

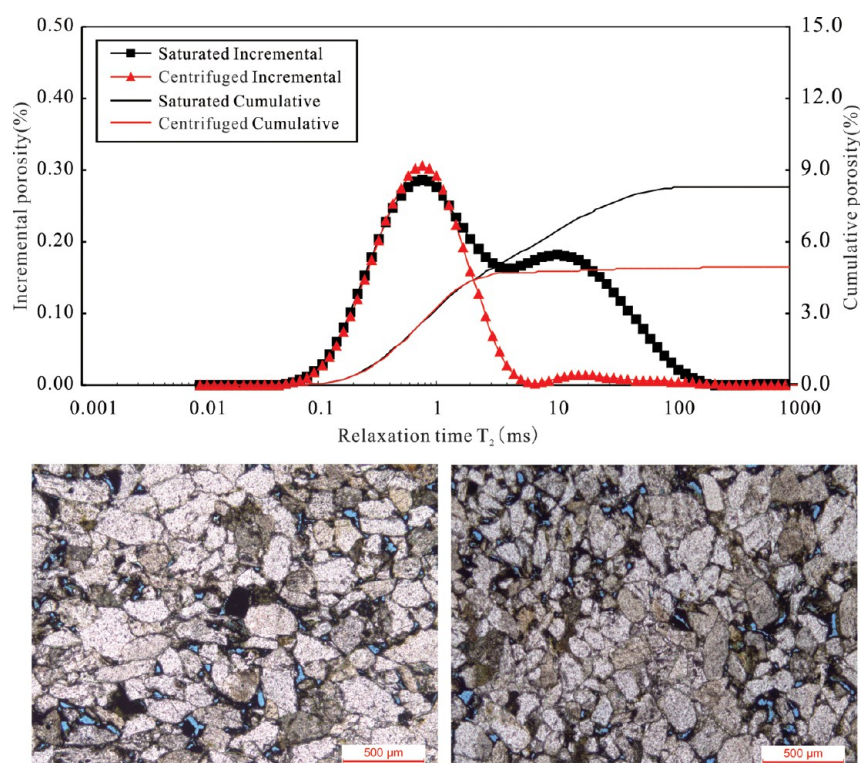


Figure 13. Typical T_2 spectrum of type C pore structure of the Sha-3 sandstones in the Raoyang sag.

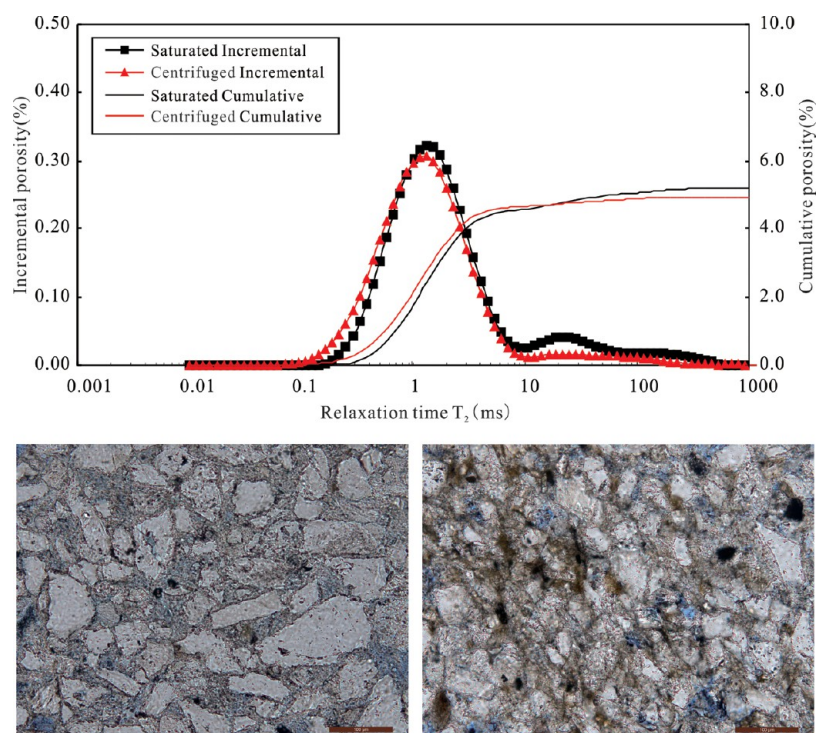


Figure 14. Typical T_2 spectrum of type D pore structure of the Sha-3 sandstones in the Raoyang sag.

maximum injection pressure, indicating poor pore connectivity, which is confirmed by the low efficiencies of mercury withdrawal.

The Sha-3 sandstones show either uni- or bimodal T_2 spectra due to the coexistence of small and large pores. Short T_2 components are commonly observed in the T_2 spectrum, and corresponding T_2 of major pore size occurs at about 1.0 to 100

ms. Capillary water and clay-bound irreducible water content is high in small pores, while the FFI is relatively low in large pores.

The NMR parameter T_{2gm} is correlated well with irreducible water saturation, core-measured permeability, and reservoir quality index. A methodology is introduced for pore structure classification and evaluation by integrating NMR parameters, e.g., T_{2gm} , BVI, and petrophysical parameters, e.g., RQI and

permeability. A total of four types of pore structures (types A, B, C, and D) are identified, while characteristics of individual pore structure are summarized using the NMR T_2 spectrum, MICP analysis, and thin-section observations.

AUTHOR INFORMATION

Corresponding Authors

*E-mail: zhangkaixun@126.com. Phone: +861-391-015-8696.

*E-mail: cugcupgych@163.com.

ORCID

Kaixun Zhang: 0000-0002-4685-7654

Notes

The authors declare no competing financial interest.

ACKNOWLEDGMENTS

We thank PetroChina Huabei Oilfield Company for providing samples and data access. This study is based on work carried out by a large group of participants. This study is supported by the National Natural Science Foundation of China (grant no. 41602152) and the Science Foundation of Chinese Academy of Geological Sciences (grant no. DZLXJK201707). The authors thank Dr. Fen Liu (a postdoctoral researcher at Research Institute of CNOOC) and Mr. Chengyu Yang (a doctoral candidate at China University of Petroleum-Beijing) for their data and technological support. The authors thank all of the researchers who have participated in the Shahejie Formation. Our deepest gratitude goes to the Prof. Jennifer Wilcox (Associate Editor of Energy & Fuels) and four anonymous reviewers for their careful work and thoughtful suggestions that have significantly improved this paper.

REFERENCES

- Jiang, Y.; Lu, H.; Liu, H. Enrichment characteristics and major controlling factors of hydrocarbons in the Neogene of Raoyang Depression, Bohai Bay Basin. *Acta Petrolei Sinica* **2011**, *32* (5), 791–796.
- Zhang, K. X.; Bai, G. P.; Jin, F. M.; Wang, Q. A. Sequence Stratigraphy-based Diagenetic Study with the Sha-3 Member sandstones in the Central-South parts of the Raoyang Depression as an Example. *Acta Petrolei Sinica* **2016**, *37* (6), 728–742.
- Mao, L.; Xiao, A.; Zhang, H.; Wu, Z.; Liufu, Y.; Wu, L.; Zhao, X. Structural patterns of the late Mesozoic crustal detachment system in the Raoyang sag, Bohai Bay basin, Eastern China: new insights from 3D seismic data. *Mar. Pet. Geol.* **2017**, *84*, 215–224.
- He, F.; Gao, X.; Zhao, X.; Yang, D.; Wang, Q.; Fan, B.; Wang, H.; Liu, J.; Wu, D. The lower part of the first member of the Shahejie formation (Es_{1x}) as a source rock for oil found in Lixian Slope, Raoyang Sag, Bohai Bay Basin, Northern China. *Arabian J. Geosci.* **2017**, *10*, 101.
- Ji, Y.; Du, J.; Zhao, X.; Zhang, Y.; Zhang, R. Sequence stratigraphy and evolution models of the Paleogene in Raoyang Sag, Jizhong Depression. *Journal of Palaeogeography* **2006**, *8* (3), 397–406 (in Chinese with English Abstract).
- Qiang, J.; Fuqi, C.; Yang, G.; Liang, C.; Chen, Z. Genetic types and accumulation models for biogenic gases in Bohai Bay Basin, Eastern China. *Bull. Can. Pet. Geol.* **2016**, *64*, 47–66.
- Cao, Y.; Zhang, H.; Xi, K.; Zhao, X.; Zhou, L.; Cui, Z.; Jin, J. Petrophysical Parameter Cutoff and Controlling Factors of Medium-Deep Effective Reservoirs of Palaeogene in Southern Raoyang Sag. *Journal of Jilin University: Earth Science Edition* **2015**, *45* (6), 1567–1579 (in Chinese with English Abstract).
- Zhang, K. X.; Bai, G. P.; Wang, Q.; Niu, X. J.; Li, Q. W.; Lu, X. X. Wireline log response-based recognition and evaluation of diagenetic facies in tight sandstone reservoirs: A case study of the Member 3 of Paleogene Shahejie Formation in Raoyang sag of Jizhong Depression. *Journal of Palaeogeography* **2016**, *18* (6), 921–938.
- Li, K.; Horne, R. N. Fractal modeling of capillary pressure curves for The Geysers rocks. *Geothermics* **2006**, *35*, 198–207.
- Hu, Q.; Ewing, R. P.; Dultz, S. Low pore connectivity in natural rock. *J. Contam. Hydrol.* **2012**, *133*, 76–83.
- Lai, J.; Wang, G. Fractal analysis of tight gas sandstones using High-Pressure Mercury Intrusion techniques. *J. Nat. Gas Sci. Eng.* **2015**, *24*, 185–196.
- Lai, J.; Wang, G.; Fan, Z.; Chen, J.; Wang, S.; Zhou, Z.; Fan, X. Insight into the pore structure of tight sandstones using NMR and HPMI measurements. *Energy Fuels* **2016**, *30*, 10200–10214.
- Xi, K.; Cao, Y.; Haile, B. G.; Zhu, R.; Jahren, J.; Bjørlykke, K.; Zhang, X.; Hellevang, H. How does the pore-throat size control the reservoir quality and oiliness of tight sandstones? The case of the Lower Cretaceous Quantou Formation in the southern Songliao Basin, China. *Mar. Pet. Geol.* **2016**, *76*, 1–15.
- Li, P.; Zheng, M.; Bi, H.; Wu, S.; Wang, X. Pore throat structure and fractal characteristics of tight oil sandstone: a case study in the Ordos basin, China. *J. Pet. Sci. Eng.* **2017**, *149*, 665–674.
- Daigle, H.; Thomas, B.; Rowe, H.; Nieto, M. Nuclear magnetic resonance characterization of shallow marine sediments from the Nankai Trough, Integrated Ocean Drilling Program Expedition 333. *Journal of Geophysical Research* **2014**, *119*, 2631–2650.
- Sigal, R. F. Pore-size distributions for organic-shale-reservoir rocks from nuclear-magnetic-resonance spectra combined with adsorption measurements. *SPE Journal* **2015**, *20*, 824–830.
- Daigle, H.; Johnson, A. Combining Mercury Intrusion and Nuclear Magnetic Resonance Measurements Using Percolation Theory. *Transp. Porous Media* **2016**, *111*, 669–679.
- Zhao, P.; Wang, Z.; Sun, Z.; Cai, J.; Wang, L. Investigation on the pore structure and multifractal characteristics of tight oil reservoirs using NMR measurements: Permian Lucaogou formation in Jimusaer sag, Junggar Basin. *Mar. Pet. Geol.* **2017**, *86*, 1067–1081.
- Lai, J.; Wang, G.; Fan, Z.; Zhou, Z.; Chen, J.; Wang, S. Fractal analysis of tight shaly sandstones using nuclear magnetic resonance measurements. *AAPG Bull.* **2018**, *102* (2), 175–193.
- Pape, H.; Clauser, C. improved interpretation of nuclear magnetic resonance T_1 and T_2 distributions for permeability prediction: simulation of diffusion coupling for a fractal cluster of pores. *Pure Appl. Geophys.* **2009**, *166*, 949–968.
- Chi, L.; Cheng, K.; Heidari, Z. Improved assessment of interconnected porosity in multiple-porosity rocks by use of Nano-particle contrast agents and nuclear-magnetic resonance relaxation measurements. *SPE Reservoir Evaluation & Engineering* **2016**, *19*, 95–107.
- Ge, X.; Fan, Y.; Zhu, X.; Chen, Y.; Li, R. Determination of nuclear magnetic resonance T_2 cutoff value based on multifractal theory - An application in sandstone with complex pore structure. *Geophysics* **2015**, *80* (1), D11–D21.
- Shao, X.; Pang, X.; Li, H.; Zhang, X. Fractal analysis of pore network in tight gas sandstones using NMR method: a case study from the Ordos basin, China. *Energy Fuels* **2017**, *31*, 10358–10368.
- Yan, J. P.; He, X.; Geng, B.; Hu, Q. H.; Feng, C. Z.; Kou, X. P.; Li, X. Nuclear magnetic resonance T_2 spectrum: multifractal characteristics and pore structure evaluation. *Applied Geophysics* **2017**, *14* (2), 205–215.
- Daigle, H.; Johnson, A.; Thomas, B. Determining fractal dimension from nuclear magnetic resonance data in rocks with internal magnetic field gradients. *Geophysics* **2014**, *79* (6), D425–D431.
- Zhou, L.; Kang, Z. Fractal characterization of pores in shales using NMR: A case study from the Lower Cambrian Niutitang Formation in the Middle Yangtze Platform, Southwest China. *J. Nat. Gas Sci. Eng.* **2016**, *35*, 860–872.
- Meng, M.; Ge, H.; Ji, W.; Wang, X. Research on the auto-removal mechanism of shale aqueous phase trapping using low field nuclear magnetic resonance technique. *J. Pet. Sci. Eng.* **2016**, *137*, 63–73.
- Rezaee, R.; Saeedi, A.; Clennell, B. Tight gas sands permeability estimation from mercury injection capillary pressure and nuclear magnetic resonance data. *J. Pet. Sci. Eng.* **2012**, *88–89*, 92–99.

- (29) Zhang, Z.; Weller, A. Fractal dimension of pore-space geometry of an Eocene sandstone formation. *Geophysics* **2014**, *79* (6), D377–D387.
- (30) Anovitz, L. M.; Cole, D. R. Characterization and analysis of porosity and pore structures. *Rev. Mineral. Geochem.* **2015**, *80* (1), 61–164.
- (31) Shao, X.; Pang, X.; Jiang, F.; Li, L.; Huyan, Y.; Zheng, D. Reservoir characterization of tight sandstones using NMR and IPMI experiments: implication for tight sand gas reservoir quality. *Energy Fuels* **2017**, *31*, 10420–10431.
- (32) Lai, J.; Wang, G.; Wang, Z.; Chen, J.; Pang, X.; Wang, S.; Zhou, Z.; He, Z.; Qin, Z.; Fan, X. A review on pore structure characterization in tight sandstones. *Earth-Sci. Rev.* **2018**, *177*, 436–457.
- (33) Schmitt, M.; Fernandes, C. P.; da Cunha Neto, J. J. A. B.; Wolf, F. G.; dos Santos, V. S. S. Characterization of pore systems in seal rocks using Nitrogen Gas Adsorption combined with Mercury Injection Capillary Pressure techniques. *Mar. Pet. Geol.* **2013**, *39*, 138–149.
- (34) Lai, J.; Wang, G.; Cao, J.; Xiao, C.; Wang, S.; Pang, X.; Dai, Q.; He, Z.; Fan, X.; Yang, L.; Qin, Z. Investigation of pore structure and petrophysical property in tight sandstones. *Mar. Pet. Geol.* **2018**, *91*, 179–189.
- (35) Feng, Y.; Jiang, S.; Hu, S.; Li, S.; Lin, C.; Xie, X. Sequence stratigraphy and importance of syndepositional structural slope-break for architecture of Paleogene syn-rift lacustrine strata, Bohai Bay basin, E. China. *Mar. Pet. Geol.* **2016**, *69*, 183–204.
- (36) Liu, Q.; He, L.; Huang, F.; Zhang, L. Cenozoic lithospheric evolution of the Bohai Bay Basin, eastern North China Craton: constraint from tectono-thermal modeling. *Journal of Asian Earth Sciences* **2016**, *115*, 368–382.
- (37) Wang, Q.; Jin, F.; Wang, S. Control factor and reservoir-forming pattern of lithologic-stratigraphic reservoirs in Raoyang Sag. *Xinjiang Petroleum Geology* **2008**, *29* (5), 595–598.
- (38) Zeng, H.; Zhao, X.; Zhu, X.; Jin, F.; Dong, Y.; Wang, Y.; Zhu, M.; Zheng, R. Seismic sedimentology characteristics of sub-clinoformal shallow-water meandering river delta: a case from the Suning area of Raoyang Sag in Jizhong depression, Bohai Bay Basin, NE China. *Petroleum Exploration and Development* **2015**, *42* (5), 621–632.
- (39) Huang, C.; Zhang, J.; Wang, H.; Jiang, S. Lacustrine shale deposition and variable tectonic accommodation in the rift basins of the Bohai Bay Basin in Eastern China. *J. Earth Sci.* **2015**, *26* (5), 700–711.
- (40) Yuan, G.; Gluyas, J.; Cao, Y.; Oxtoby, N. H.; Jia, Z.; Wang, Y.; Xi, K.; Li, X. Diagenesis and reservoir quality evolution of the Eocene sandstones in the northern Dongying Sag, Bohai Bay Basin, East China. *Mar. Pet. Geol.* **2015**, *62*, 77–89.
- (41) Guo, X.; He, S.; Liu, K.; Shi, Z.; Bachir, S. Modelling the petroleum generation and migration of the third member of the Shahejie Formation (Es3) in the Banqiao Depression of Bohai Bay Basin, Eastern China. *Journal of Asian Earth Sciences* **2011**, *40*, 287–302.
- (42) Yuan, G.; Cao, Y.; Gluyas, J.; Li, X.; Xi, K.; Wang, Y.; Jia, Z.; Sun, P.; Oxtoby, N. H. Feldspar dissolution, authigenic clays, and quartz cements in open and closed sandstone geochemical systems during diagenesis: Typical examples from two sags in Bohai Bay Basin, East China. *AAPG Bull.* **2015**, *99* (11), 2121–2154.
- (43) Kassab, M. A.; Abu Hashish, M. F.; Nabawy, B. S.; Elnaggar, O. M. Effect of kaolinite as a key factor controlling the petrophysical properties of the Nubia sandstone in central Eastern desert, Egypt. *J. Afr. Earth Sci.* **2017**, *125*, 103–117.
- (44) Freiburg, J. T.; Ritz, R. W.; Kehoe, K. S. Depositional and diagenetic controls on anomalously high porosity within a deeply buried CO₂ storage reservoir—the Cambrian Mt. Simon sandstone, Illinois basin, USA. *Int. J. Greenhouse Gas Control* **2016**, *55*, 42–54.
- (45) Dutton, S. P.; Loucks, R. D. Diagenetic controls on evolution of porosity and permeability in lower Tertiary Wilcox sandstones from shallow to ultradeep (200–6700 m) burial, Gulf of Mexico Basin, U.S.A. *Mar. Pet. Geol.* **2010**, *27*, 69–81.
- (46) Li, K. Analytical derivation of Brooks–Corey type capillary pressure models using fractal geometry and evaluation of rock heterogeneity. *J. Pet. Sci. Eng.* **2010**, *73*, 20–26.
- (47) Torabi, A.; Fossen, H.; Braathen, A. Insight into petrophysical properties of deformed sandstone reservoirs. *AAPG Bull.* **2013**, *97* (4), 619–637.
- (48) Nooruddin, H. A.; Hossain, M. E.; Al-Yousef, H.; Okasha, T. Comparison of permeability models using mercury injection capillary pressure data on carbonate rock samples. *J. Pet. Sci. Eng.* **2014**, *121*, 9–22.
- (49) Sakhaee-Pour, A.; Bryant, S. L. Effect of pore structure on the producibility of tight-gas sandstones. *AAPG Bull.* **2014**, *98* (4), 663–694.
- (50) Xiao, D.; Lu, Z.; Jiang, S.; Lu, S. Comparison and integration of experimental methods to characterize the full-range pore features of tight gas sandstone—a case study in Songliao basin of China. *J. Nat. Gas Sci. Eng.* **2016**, *34*, 1412–1421.
- (51) Schmitt, M.; Fernandes, C. P.; Wolf, F. G.; da Cunha Neto, J. A. B.; Rahner, C. P.; dos Santos, V. S. S. Characterization of Brazilian tight gas sandstones relating permeability and angstrom-to micron-scale pore structures. *J. Nat. Gas Sci. Eng.* **2015**, *27*, 785–807.
- (52) Müller-Huber, E.; Schön, J.; Börner, F. Pore space characterization in carbonate rocks—Approach to combinenuclear magnetic resonance and elastic wave velocity measurements. *Journal of Applied Geophysics* **2016**, *127*, 68–81.
- (53) Dillinger, A.; Esteban, L. Experimental evaluation of reservoir quality in Mesozoic formations of the Perth Basin (Western Australia) by using a laboratory low field Nuclear Magnetic Resonance. *Mar. Pet. Geol.* **2014**, *57*, 455–469.
- (54) Gao, H.; Li, H. Determination of movable fluid percentage and movable fluid porosity in ultra-low permeability sandstone using nuclear magnetic resonance (NMR) technique. *J. Pet. Sci. Eng.* **2015**, *133*, 258–267.
- (55) Chi, L.; Heidari, Z. Diffusional coupling between microfractures and pore structure and its impact on nuclear magnetic resonance measurements in multiple-porosity systems. *Geophysics* **2015**, *80* (1), D31–D42.
- (56) Zou, C.; Zhu, R.; Liu, K.; Su, L.; Bai, B.; Zhang, X.; Yuan, X.; Wang, J. Tight gas sandstone reservoirs in China: characteristics and recognition criteria. *J. Pet. Sci. Eng.* **2012**, *88–89*, 82–91.
- (57) Zhao, H.; Ning, Z.; Zhao, T.; Zhang, R.; Wang, Q. Effects of mineralogy on petrophysical properties and permeability estimation of the Upper Triassic Yanchang tight oil sandstones in Ordos Basin, Northern China. *Fuel* **2016**, *186*, 328–338.
- (58) Zhang, L.; Lu, S.; Xiao, D.; Li, B. Pore structure characteristics of tight sandstones in the Northern Songliao basin, China. *Mar. Pet. Geol.* **2017**, *88*, 170–180.
- (59) Wang, H.; Liu, Y.; Song, Y.; Zhao, Y.; Zhao, J.; Wang, D. Fractal analysis and its impact factors on pore structure of artificial cores based on the images obtained using magnetic resonance imaging. *Journal of Applied Geophysics* **2012**, *86*, 70–81.
- (60) Lai, J.; Wang, G.; Chen, M.; Wang, S.; Chai, Y.; Cai, C.; Li, J.; Zhang, Y. Pore structures evaluation of low permeability clastic reservoirs based on petrophysical facies: A case study on Chang 8 reservoir in the Jiyuan region, Ordos Basin. *Petroleum Exploration and Development* **2013**, *40* (5), 606–614.
- (61) Coates, G. R.; Peveraro, R. C. A.; Hardwick, A.; Roberts, D. The magnetic resonance imaging log characterized by comparison with petrophysical properties and laboratory core data. In *Proceedings of the 66th Annual Technical Conference and Exhibition, Formation Evaluation and Reservoir Geology*; Society of Petroleum Engineers: Richardson, TX, 1991; pp 627–635.
- (62) Tavakoli, V.; Rahimpour-Bonab, H.; Esrafil-Dizaji, B. Diagenetic controlled reservoir quality of South Pars gas field, an integrated approach. *C. R. Geosci.* **2011**, *343*, 55–71.
- (63) Lai, J.; Wang, G.; Chai, Y.; Ran, Y.; Zhang, X. Depositional and diagenetic controls on reservoir pore structure of tight gas sandstones: evidence from Lower Cretaceous Bashijiqike Formation in Kelasu Thrust belts, Kuqa depression in Tarim Basin of West China. *Resour. Geol.* **2015**, *65* (2), 55–75.
- (64) Amaefule, J. O.; Mehmet, A.; Djebbar, T.; David, K.; Dare, K. Enhanced reservoir description: using core and log data to identify

hydraulic (flow) unit and predict permeability in uncored intervals/well. In *Proceedings of the 68th Annual SPE Conference and Exhibition*; Society of Petroleum Engineers: Houston, TX, 1993.

(65) Pittman, E. D. Relationship of porosity and permeability to various parameters derived from mercury injection-capillary pressure curves for sandstones. *AAPG Bull.* **1992**, *76*, 191–198.

(66) Bloch, S.; Lander, R. H.; Bonnell, L. Anomalously high porosity and permeability in deeply buried sandstone reservoirs: Origin and predictability. *AAPG Bull.* **2002**, *86* (2), 301–328.